International Journal of Thermal Sciences 54 (2012) 98–108

Contents lists available at SciVerse ScienceDirect

International Journal of Thermal Sciences

journal homepage: www.elsevier.com/locate/ijts

Heat transfer performance assessment for forced convection in a tube partially filled with a porous medium

Chen Yang [a,b,*], Akira Nakayama [a,c,1], Wei Liu [b]

[a] Department of Mechanical Engineering, Shizuoka University, 3-5-1 Johoku, Naka-Ku, Hamamatsu 432-8561, Japan
[b] School of Energy and Power Engineering, Huazhong University of Science and Technology, Wuhan, Hubei 430074, PR China
[c] School of Civil Engineering and Architecture, Wuhan Polytechnic University, Wuhan, Hubei 430023, PR China

ARTICLE INFO

Article history:
Received 29 July 2011
Received in revised form
27 October 2011
Accepted 29 October 2011
Available online 1 December 2011

Keywords:
Porous media
Thermal non-equilibrium
Pumping power
Metal foam
Heat transfer performance

ABSTRACT

Heat transfer performance assessment was made for forced convection in a heated tube with a porous medium core and a tube with a wall covered with a porous medium layer, so as to investigate effectiveness of porous material insertion within a tube. Both local thermal and non-thermal equilibrium analyses were carried out for the two cases of partial porous medium filling, to investigate the validity of local thermal equilibrium assumption. It has been found that the local thermal non-equilibrium analysis is essential for the case of forced convection in a tube with a heated wall surface covered with a porous medium layer, whereas the local thermal equilibrium analysis suffices to capture transport phenomena for the case of forced convection in a tube with a porous medium core. In a comparatively low range of pumping power, the heat transfer performance of the tube with a porous medium core is higher than that of the tube with a wall covered with a porous medium layer. However, in a high range of pumping power, the latter performance exceeds the former.

1. Introduction

The utilization of porous medium inside the tube has attracted considerable attention due to its possible potential in enhancing heat transfer performance, such as in solid matrix heat exchangers, fuel cells, electronic devices, solar absorbers, and so on. A comprehensive literature review associated with partial filling of porous medium inside the tube can be found in Ref. [1].

A number of researchers dealt with the Brinkman effects on the velocity profile in the tube. As pointed out by Dukhan et al. [2], the Darcian velocity shows its dependence on the transverse direction only in a small region very close to the wall. Base on the plug flow approximation, they carried out a simple heat analysis and obtained approximate solutions, which agree very well with the corresponding experimental results. A theoretical study of fully developed forced convection in a channel filled with a porous matrix was presented by Poulikakos and Kazmierczak [3]. They concluded that the Brinkman flow model is appropriate only for the flows in sparsely packed porous media.

Many researchers [4–17] focused on the two-energy equation models based on the assumption of local thermal non-equilibrium, because the assumption of local thermal equilibrium often fails, for the cases, in which there is large difference between the thermal conductivities of fluid and solid phases, or significant heat generation in any one of the phases. Nakayama et al. [18] used the two-energy equation model introduced by Hsu [19] and Hsu et al. [20], and obtained exact solutions for two fundamental steady heat transfer cases, namely, one-dimensional steady heat conduction in a porous slab with internal heat generation, and also thermally developing unidirectional flow through a semi-infinite porous medium. They pointed out that the thermal equilibrium assumption ceases to be valid even for certain steady thermal problems.

Tong et al. [21] conducted a series of numerical calculations for a channel with its core partially filled with a porous medium. They claimed that for some conditions heat transfer is maximized by using a porous medium thinner than the channel height. Based on the assumption of local thermal equilibrium, Yang et al. [22] obtained the analytical solutions for fluid flow and heat transfer, and elucidated the existence of the optimal porous core diameter ratio, which yields the maximum heat transfer coefficient. Bhargavi and Satyamurty [23] considered three different arrangements of porous media in parallel plate channels subject to uniform heat flux. It has been found that partial filling of porous medium in the core region yields the maximum enhancement in heat transfer per unit pressure

* Corresponding author. Department of Mechanical Engineering, Shizuoka University, 3-5-1 Johoku, Naka-Ku, Hamamatsu 432-8561, Japan. Tel./fax: +81 53 478 1049.
E-mail address: f5945037@ipc.shizuoka.ac.jp (C. Yang).
[1] Tel./fax: +81 53 478 1049.

1290-0729/$ – see front matter © 2011 Elsevier Masson SAS. All rights reserved.
doi:10.1016/j.ijthermalsci.2011.10.023

gradient. In light of the Darcy–Brinkman law and the assumption of local thermal non-equilibrium, Xu et al. [24] derived the exact solutions for both fluid and solid phases. Meanwhile, a parametric study was performed to investigate the influences of various factors on the flow resistance and heat transfer performance. Pavel and Mohamad [25,26], Mohamad [27] and Huang et al. [28] performed the corresponding experimental investigations for the partial filling of porous medium inserts in the core region of tube. They claim that the porous medium inserts are effective to enhance heat transfer at expense of a reasonable pressure drop.

In the previous investigations, however, the effects of local thermal non-equilibrium assumption on heat transfer in tubes with porous media insertions have not been sufficiently elucidated yet. In this study, firstly, we shall consider forced convection in a tube with a porous medium core and a tube with a wall covered with a porous medium layer. These two ways of porous media insertions may lead to possible increase in heat transfer rates at a reasonable increase of pressure drop. Both local thermal and non-thermal equilibrium analyses will be made for the two cases to investigate the validity of local thermal equilibrium assumption. Secondly, we shall investigate effectiveness of porous material insertion within a tube, so as to find out where in a tube to place porous media, either in the core or over the wall. It will be found that, in a low range of pumping power, the heat transfer performance of the tube with a porous medium core is higher than that of the tube with a wall covered with a porous medium layer. However, in a high range of pumping power, the latter performance exceeds the former.

2. Mathematical model based on local thermal non-equilibrium assumption

Upon integrating two energy equations for the two individual phases over a representative elementary volume V following the volume averaging theory [29–32], we obtain the macroscopic energy equations for the two individual phases as follows:

For the fluid phase:

$$\varepsilon\rho_f c_{p_f}\frac{\partial\langle T\rangle^f}{\partial t}+\varepsilon\rho_f c_{p_f}\frac{\partial\langle u_j\rangle^f\langle T\rangle^f}{\partial x_j}=\frac{\partial}{\partial x_j}\left(\varepsilon k_f\frac{\partial\langle T\rangle^f}{\partial x_j}+\frac{k_f}{V}\int_{A_{int}}Tn_j dA-\rho_f c_{p_f}\varepsilon\left\langle\tilde{u}_j\tilde{T}\right\rangle^f\right)+\frac{1}{V}\int_{A_{int}}k_f\frac{\partial T}{\partial x_j}n_j dA \quad (1)$$

For the solid matrix phase:

$$\rho_s c_s(1-\varepsilon)\frac{\partial\langle T\rangle^s}{\partial t}=\frac{\partial}{\partial x_j}\left((1-\varepsilon)k_s\frac{\partial\langle T\rangle^s}{\partial x_j}-\frac{k_s}{V}\int_{A_{int}}Tn_j dA\right)-\frac{1}{V}\int_{A_{int}}k_f\frac{\partial T}{\partial x_j}n_j dA \quad (2)$$

where the volume average of a certain variable ϕ in the fluid phase is defined as

$$\langle\phi\rangle^f\equiv\frac{1}{V_f}\int_{V_f}\phi dV$$

such that $\langle T\rangle^f$ is the intrinsic volume average of the fluid temperature, while $\langle T\rangle^s$ is the intrinsic volume average of the solid matrix temperature, where V_f is the volume space which the fluid phase occupies. The porosity $\varepsilon\equiv V_f/V$ is the volume fraction of the fluid space. The variable ϕ is decomposed into its intrinsic average and the spatial deviation from it:

$$\phi=\langle\phi\rangle^f+\tilde{\phi}$$

Moreover, A_{int} is the local interfacial area between the fluid and solid matrix, while n_i is the unit vector pointing outward from the fluid side to solid side. The continuity of both temperature and heat flux is imposed on the interface. Obviously, the parenthetical terms on the right hand-side of Eq. (1) denote the diffusive heat transfer, while the last term describes the interfacial heat transfer between the solid and fluid phases. In terms of the local thermal equilibrium assumption, the following one-equation model can be achieved by combining the previous Eqs. (1) and (2):

$$\left(\varepsilon\rho_f c_{p_f}+(1-\varepsilon)\rho_s c_s\right)\frac{\partial\langle T\rangle}{\partial t}+\rho_f c_{p_f}\frac{\partial\langle u_j\rangle\langle T\rangle}{\partial x_j}=\frac{\partial}{\partial x_j}\left(\left(\varepsilon k_f+(1-\varepsilon)k_s\right)\frac{\partial\langle T\rangle}{\partial x_j}+\frac{k_f-k_s}{V}\int_{A_{int}}Tn_j dA-\varepsilon\rho_f c_{p_f}\left\langle\tilde{u}_j\tilde{T}\right\rangle^f\right) \quad (3)$$

where

$$\langle\phi\rangle\equiv\frac{1}{V}\int_V\phi dV$$

is the Darcian average of the variable ϕ such that $\langle u_j\rangle=\varepsilon\langle u_j\rangle^f$ is the Darcian velocity vector. From the foregoing Eq. (3), the macroscopic heat flux vector $q_i=(q_x,q_y,q_z)$ and its corresponding stagnant thermal conductivity k_{stag} may be defined as follows:

$$q_i=-k_{stag}\frac{\partial\langle T\rangle}{\partial x_i}+\varepsilon\rho_f c_{p_f}\left\langle\tilde{u}_i\tilde{T}\right\rangle^f=-\left(\varepsilon k_f+(1-\varepsilon)k_s\right)\frac{\partial\langle T\rangle}{\partial x_i}-\left(k_f-k_s\right)\frac{1}{V}\int_{A_{int}}Tn_i dA+\varepsilon\rho_f c_{p_f}\left\langle\tilde{u}_i\tilde{T}\right\rangle^f \quad (4)$$

Note that the first term in the rightmost expression corresponds to the upper bound of the effective stagnant thermal conductivity based on the parallel model, namely, $(\varepsilon k_f+(1-\varepsilon)k_s)$. Thus, it is the tortuosity term (i.e. the second term) that adjusts the level of the effective stagnant thermal conductivity from its upper bound to a correct one.

Meanwhile, for obtaining more concise forms of the previous two energy equations, the following two-energy equation model was presented by Yang and Nakayama [33] along with the effective porosity:

For the fluid phase:

$$\rho_f c_{p_f}\varepsilon\frac{\partial\langle T\rangle^f}{\partial t}+\rho_f c_{p_f}\frac{\partial\langle u_j\rangle\langle T\rangle^f}{\partial x_j}=\frac{\partial}{\partial x_j}\left(\left(\varepsilon^* k_f\frac{\partial\langle T\rangle^f}{\partial x_j}+\varepsilon k_{dis_{jk}}\frac{\partial\langle T\rangle^f}{\partial x_k}\right)\right)-h_v\left(\langle T\rangle^f-\langle T\rangle^s\right) \quad (5)$$

For the solid matrix phase:

$$\rho_s c_s(1-\varepsilon)\frac{\partial\langle T\rangle^s}{\partial t}=\frac{\partial}{\partial x_j}\left(\left(1-\varepsilon^*\right)k_s\frac{\partial\langle T\rangle^s}{\partial x_j}\right)-h_v\left(\langle T\rangle^s-\langle T\rangle^f\right) \quad (6)$$

where the effective porosity ε^* which accounts for the effect of tortuosity on the stagnant thermal conductivity is defined such that the stagnant thermal conductivity is given by

$$k_{\mathrm{stag}} = \varepsilon^* k_{\mathrm{f}} + \left(1-\varepsilon^*\right)k_{\mathrm{s}} \tag{7a}$$

namely,

$$\varepsilon^* = \frac{k_{\mathrm{s}}-k_{\mathrm{stag}}}{k_{\mathrm{s}}-k_{\mathrm{f}}} = \varepsilon + \frac{\varepsilon k_{\mathrm{f}} + (1-\varepsilon)k_{\mathrm{s}} - k_{\mathrm{stag}}}{k_{\mathrm{s}}-k_{\mathrm{f}}} \tag{7b}$$

such that Eq. (4) gives

$$\left(\varepsilon^*-\varepsilon\right)\frac{\partial\langle T\rangle}{\partial x_{\mathrm{i}}} = \frac{1}{V}\int\limits_{A_{\mathrm{int}}} T n_{\mathrm{i}}\,\mathrm{d}A \tag{8}$$

As the stagnant thermal conductivity k_{stag} is given either empirically or theoretically, the effective porosity ε^* can easily be evaluated from (7b). Furthermore, the thermal dispersion term is modeled according to the gradient diffusion hypothesis [34]:

$$-\rho_{\mathrm{f}} c_{\mathrm{p_f}}\left\langle \tilde{u}_{\mathrm{j}}\tilde{T}\right\rangle^{\mathrm{f}} = k_{\mathrm{dis_{kj}}}\frac{\partial\langle T\rangle^{\mathrm{f}}}{\partial x_{\mathrm{k}}} \tag{9}$$

while the interfacial heat transfer between the solid and fluid phases is modeled using Newton's cooling law:

$$\frac{1}{V}\int\limits_{A_{\mathrm{int}}} k_{\mathrm{f}}\frac{\partial T}{\partial x_{\mathrm{j}}} n_{\mathrm{j}}\,\mathrm{d}A = h_{\mathrm{v}}\left(\langle T\rangle^{\mathrm{s}} - \langle T\rangle^{\mathrm{f}}\right) \tag{10}$$

where h_{v} is the volumetric heat transfer coefficient, which must be prescribed.

3. Physical model and its velocity field

First, we consider the fluid flow and heat transfer in a tube with its wall covered with a porous medium layer. As indicated in Fig. 1(a), the tube whose wall is entirely covered by a metal foam layer is long enough for both velocity and temperature fields to be fully developed. The wall is subject to a constant and uniform heat flux.

Xu et al. [24] carried out a local thermal non-equilibrium analysis using their two equation model which is equivalent to the present model, but without consideration of tortuosity. They used

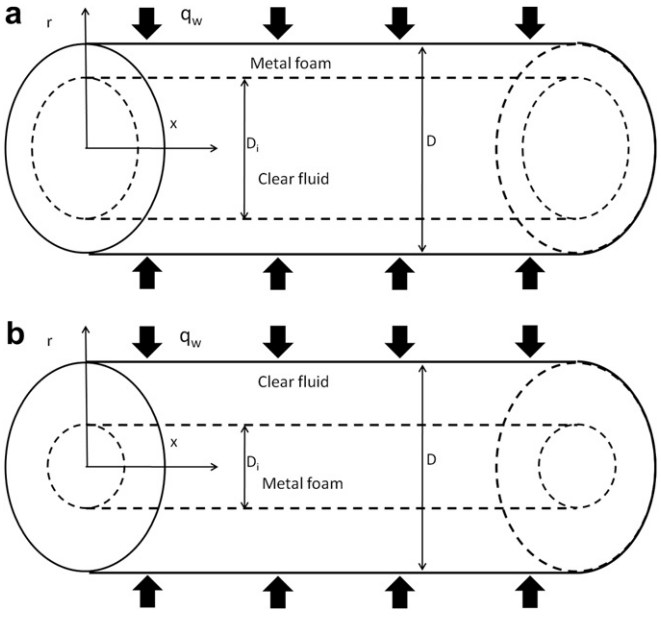

Fig. 1. (a) A tube with its wall covered with a porous medium layer. (b) A tube with a porous medium core.

the Brinkman extended Darcy velocity profile to obtain individual temperature profiles for fluid and solid phases. However, they never compared their results with those obtained under the local thermal equilibrium assumption. Thus, we shall carry out both local thermal equilibrium and non-equilibrium analyses to compare both sets of the results, to examine possible limitations of the local thermal equilibrium assumption.

Although the exact temperature profiles obtained by Xu et al. [24] with the Brinkman extended Darcy velocity profile are available, they are quite complex and formidable to use for heat transfer estimations. Thus, we shall seek the approximate temperature profiles exploiting the plug flow approximation. As pointed out by Dukhan et al. [2], the Darcian velocity shows its dependence on the transverse direction only in a small region very close to the wall. Its effects are so minor to reflect on the corresponding temperature profiles. This will shortly be confirmed below by comparing our results based on the plug flow against those of Xu et al. [24].

Based on the Darcy's law, we assume the plug flow within a porous layer adjacent to the wall and obtain:

$$u = -\frac{K}{\mu_{\mathrm{f}}}\frac{d\langle p\rangle^{\mathrm{f}}}{dx} \equiv u_i = \text{const.} \quad \text{for} \quad D_{\mathrm{i}}/2 \le r \le D/2 \tag{11}$$

whereas the interfacial hydrodynamics compatibility conditions at $r = D_{\mathrm{i}}/2$ are given by:

$$\begin{aligned} &u|_{(r-D_{\mathrm{i}}/2)\to -0} = u|_{(r-D_{\mathrm{i}}/2)\to +0}, \\ &\mu_{\mathrm{f}}\frac{\partial u}{\partial r}\Big|_{(r-D_{\mathrm{i}}/2)\to -0} = \frac{\mu_{\mathrm{f}}}{\varepsilon}\frac{\partial u}{\partial r}\Big|_{(r-D_{\mathrm{i}}/2)\to +0} \end{aligned} \tag{12}$$

Subsequently, the velocity profile within the fluid region may readily be determined as:

$$u = -\frac{u_{\mathrm{i}}}{16\mathrm{Da}}\left(\frac{r}{D/2}\right)^2 + u_{\mathrm{i}}\left[1+\frac{R_{\mathrm{p}}}{16\mathrm{Da}}\right] \quad \text{for} \quad 0 \le r \le D_{\mathrm{i}}/2 \tag{13}$$

where $\mathrm{Da} = K/D^2$ is the Darcy number whereas $R_{\mathrm{p}} = D_{\mathrm{i}}/D$ is the inner and outer diameter ratio. In light of mass conservation in the cross section of a tube, the interfacial velocity u_{i} is related to the bulk mean velocity u_{B} in the tube as:

$$\frac{u_{\mathrm{i}}}{u_{\mathrm{B}}} = \frac{32\mathrm{Da}}{32\mathrm{Da}+R_{\mathrm{p}}^4} \tag{14}$$

Furthermore, for a given set of Reynolds number $\mathrm{Re_D}$ and R_{p}, the friction factor λ_{f} may readily be obtained as:

$$\lambda_{\mathrm{f}} \equiv -\frac{2D}{\rho u_{\mathrm{B}}^2}\frac{\mathrm{d}\langle p\rangle^{\mathrm{f}}}{\mathrm{d}x} = \frac{64}{\mathrm{Re_D}\left(32\mathrm{Da}+R_{\mathrm{p}}^4\right)} \tag{15}$$

In Figs. 2 and 3, the present velocity profiles based on the plug flow approximation are compared with those obtained by Xu et al. with the Brinkman term for three porous diameter ratios, namely, 0.1, 0.3 and 0.5, respectively. It is clearly seen from the figures that for the large Darcy number such as in the case of $\mathrm{Da} = 10^{-3}$, the Brinkman effects on the velocity are significant, while, for the relatively low Darcy number such as in the case of $\mathrm{Da} = 1.5\times10^{-4}$, the effects on the velocity diminish such that the Brinkman term in the momentum equation of porous medium may well be neglected for simplicity.

4. Thermal analysis for forced convection in a tube with its wall covered with a porous medium layer

For relatively small Darcy number, the neglect of Brinkman term in the momentum equation of porous media would not result in serious errors. Therefore, we may neglect the boundary term (i.e.

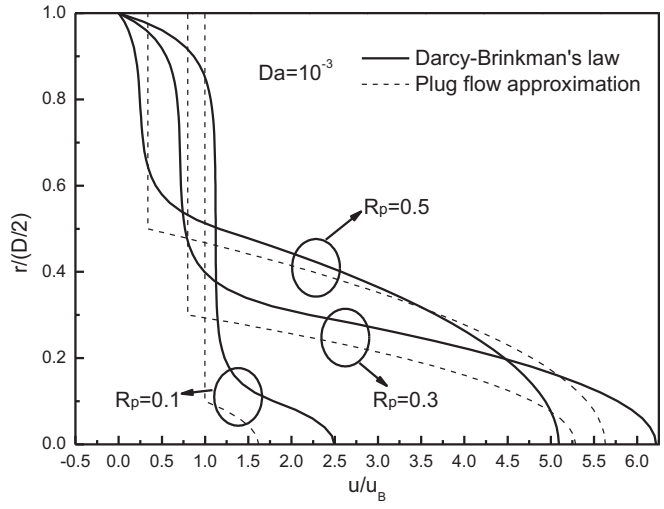

Fig. 2. The velocity profiles for the case of $Da = 10^{-3}$.

Brinkman term) and use the plug flow approximation. The experimental investigations performed by Jamin and Mohamad [35] indicate that the contact resistance between the heating wall and porous medium may have significant effect on the heat transfer performance. However, for simplification, the effect of contact resistance is neglected in this study. In what follows, we shall present the thermal non-equilibrium analysis, which will be followed by the thermal equilibrium version.

4.1. Local thermal non-equilibrium analysis

Under the plug flow approximation, the energy equations for the fluid phase and solid phase in a porous medium region are given as following:

$$\rho_f c_{p_f} u_D \frac{\partial \langle T\rangle^f}{\partial x} = \left(\varepsilon^* k_f + \varepsilon k_{dis_{yy}}\right)\frac{1}{r}\frac{\partial}{\partial r}\left(r\frac{\partial \langle T\rangle^f}{\partial r}\right) - h_v\left(\langle T\rangle^f - \langle T\rangle^s\right) \tag{16}$$

and

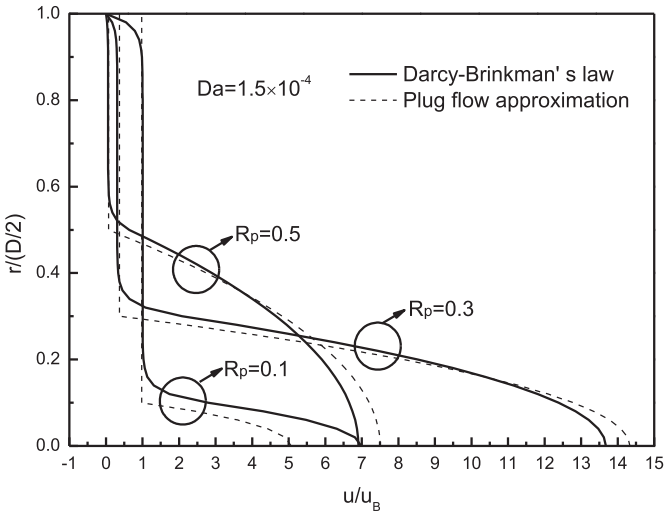

Fig. 3. Velocity profiles for the case of $Da = 1.5 \times 10^{-4}$.

$$\left(1-\varepsilon^*\right)k_s\frac{1}{r}\frac{\partial}{\partial r}\left(r\frac{\partial \langle T\rangle^s}{\partial r}\right) - h_v\left(\langle T\rangle^s - \langle T\rangle^f\right) = 0 \tag{17}$$

Meanwhile, the energy equation in the clear fluid region is:

$$\rho_f c_{p_f} u \frac{\partial \langle T\rangle^f}{\partial x} = \frac{k_f}{r}\frac{\partial}{\partial r}\left(r\frac{\partial \langle T\rangle^f}{\partial r}\right) \tag{18}$$

whereas the interfacial thermal compatibility conditions at $r = D_i/2$ are given by:

$$\begin{aligned} &\langle T\rangle^f|_{(r-D_i/2)\to -0} = \langle T\rangle^f|_{(r-D_i/2)\to +0}, \\ &k_f\frac{\partial \langle T\rangle^f}{\partial r}\Big|_{(r-D_i/2)\to -0} = \left(\varepsilon^* k_f + \varepsilon k_{dis_{yy}}\right)\frac{\partial \langle T\rangle^f}{\partial r}\Big|_{(r-D_i/2)\to +0} \end{aligned} \tag{19}$$

Eqs. (16) and (17) are added to form

$$\rho_f c_{p_f} u_D \frac{\partial \langle T\rangle^f}{\partial x} = \frac{1}{r}\frac{\partial}{\partial r}\left(\left(\varepsilon^* k_f + \varepsilon k_{dis_{yy}}\right) r\frac{\partial \langle T\rangle^f}{\partial r} + \left(1-\varepsilon^*\right)k_s r\frac{\partial \langle T\rangle^s}{\partial r}\right) \tag{20}$$

where

$$J \equiv \frac{u_D}{u_B} = \frac{u_i}{u_B} = \frac{32Da}{32Da + R_p^4} \tag{21}$$

The energy balance for the case of constant heat flux readily gives:

$$\left(\frac{\pi D^2}{4}\right)\rho_f c_{p_f} u_B \frac{d\langle T\rangle_B^f}{dx} = (\pi D) q_w \tag{22}$$

where $\langle T\rangle_B^f$ is the bulk temperature of the fluid phase. Since $d\langle T\rangle_B^f/dx = \partial\langle T\rangle^f/\partial x$, Eqs. (16) and (18) can be rewritten as follows:

$$\frac{4q_w}{D}\frac{u_D}{u_B} = \left(\varepsilon^* k_f + \varepsilon k_{dis_{yy}}\right)\frac{1}{r}\frac{\partial}{\partial r}\left(r\frac{\partial \langle T\rangle^f}{\partial r}\right) - h_v\left(\langle T\rangle^f - \langle T\rangle^s\right) \tag{23}$$

and

$$\frac{4q_w}{D}\frac{u}{u_B} = \frac{k_f}{r}\frac{\partial}{\partial r}\left(r\frac{\partial \langle T\rangle^f}{\partial r}\right) \tag{24}$$

Correspondingly, Eq. (20) can be transformed as

$$\frac{1}{r}\frac{\partial}{\partial r}\left(\left(\varepsilon^* k_f + \varepsilon k_{dis_{yy}}\right) r\frac{\partial \langle T\rangle^f}{\partial r} + \left(1-\varepsilon^*\right)k_s r\frac{\partial \langle T\rangle^s}{\partial r}\right) = 4\frac{q_w}{D}J$$

This may be integrated as

$$\left(\varepsilon^* k_f + \varepsilon k_{dis_{yy}}\right)\frac{\partial \langle T\rangle^f}{\partial r} + \left(1-\varepsilon^*\right)k_s\frac{\partial \langle T\rangle^s}{\partial r} = \frac{q_w D}{2}\left(4J\frac{r}{D^2} + \frac{1-J}{r}\right)$$

where the boundary condition $q_w = (\varepsilon^* k_f + \varepsilon k_{dis_{yy}})(\partial\langle T\rangle^f/\partial r)|_{r=D/2} + (1-\varepsilon^*)k_s(\partial\langle T\rangle^s/\partial r)|_{r=D/2} = \text{const.}$ is exploited. The equation can further be integrated as

$$\begin{aligned} &\left(\varepsilon^* k_f + \varepsilon k_{dis_{yy}}\right)\left((T_w - \Delta T) - \langle T\rangle^f\right) + \left(1-\varepsilon^*\right)k_s\left(T_w - \langle T\rangle^s\right) \\ &= \frac{q_w D}{2}\left[2J\left(\frac{1}{4} - \frac{r^2}{D^2}\right) + (J-1)\ln\frac{r}{D/2}\right] \end{aligned} \tag{25}$$

where $\langle T\rangle^s|_{r=D/2} = T_w$ and $\langle T\rangle^f|_{r=D/2} = T_w - \Delta T$. The degree of thermal non-equilibrium, $\Delta T = (\langle T\rangle^s - \langle T\rangle^f)|_{r=D/2}$, must be prescribed. As pointed out by Yang et al. [36], when

$\Delta T = (\langle T\rangle^{s} - \langle T\rangle^{f})|_{r=D/2}$ is equal to zero, the results are expected to be closer to the reality. The foregoing relationship (25) between the solid and fluid temperatures is substituted into Eq. (17) to obtain the following ordinary differential equation in terms of $(\langle T\rangle^{s} - T_w)$ as

$$\left(1-\varepsilon^*\right)k_s\frac{1}{r}\frac{d}{dr}\left(r\frac{d\left(\langle T\rangle^{s}-T\right)}{\partial r}\right)-\frac{k_{stag}+\varepsilon k_{dis_{yy}}}{\varepsilon^* k_f+\varepsilon k_{dis_{yy}}}h_v\left(\langle T\rangle^{s}-T_w\right) = \frac{h_v q_w D}{2\left(\varepsilon^* k_f+\varepsilon k_{dis_{yy}}\right)}\left(2J\left(\frac{1}{4}-\frac{r^2}{D^2}\right)+(J-1)\ln\frac{r}{D/2}\right) \tag{26}$$

Note that $(\langle T\rangle^{s} - T_w)$ is a function of r alone, since $dT_w/dx = 4q_w/\rho_f c_{p_f} u_B D$. This ordinary differential equation, after some manipulations, yields

$$\frac{\langle T\rangle^{s}-T_w}{Dq_w/\left(k_{stag}+\varepsilon k_{dis_{yy}}\right)} = L_1 I_0(\lambda r)+L_2 K_0(\lambda r) + M_1\left(\frac{r}{D}\right)^2+M_2\ln\frac{r}{D/2}+M_3 \tag{27}$$

where

$$L_1 = \frac{-\left(M_1\frac{R_p^2}{2}+M_2\right)K_0(\lambda D/2)+\left(\frac{M_1}{4}+M_3\right)\frac{D_i}{2}\left.\frac{dK_0(\lambda r)}{dr}\right|_{r=\frac{D_i}{2}}}{K_0(\lambda D/2)\frac{D_i}{2}\left.\frac{dI_0(\lambda r)}{dr}\right|_{r=\frac{D_i}{2}}-I_0(\lambda D/2)\frac{D_i}{2}\left.\frac{dK_0(\lambda r)}{dr}\right|_{r=\frac{D_i}{2}}} \tag{28}$$

$$L_2 = \frac{-\left(M_1\frac{R_p^2}{2}+M_2\right)I_0(\lambda D/2)+\left(\frac{M_1}{4}+M_3\right)\frac{D_i}{2}\left.\frac{dI_0(\lambda r)}{dr}\right|_{r=\frac{D_i}{2}}}{I_0(\lambda D/2)\frac{D_i}{2}\left.\frac{dK_0(\lambda r)}{dr}\right|_{r=\frac{D_i}{2}}-K_0(\lambda D/2)\frac{D_i}{2}\left.\frac{dI_0(\lambda r)}{dr}\right|_{r=\frac{D_i}{2}}} \tag{29}$$

$$M_1 = J \tag{30}$$

$$M_2 = \frac{1-J}{2} \tag{31}$$

$$M_3 = \frac{4J}{(\lambda D)^2}-\frac{J}{4} \tag{32}$$

$$\lambda = \sqrt{\frac{\left(\frac{k_{stag}}{k_f}+\varepsilon\frac{k_{dis_{yy}}}{k_f}\right)}{\left(\varepsilon^*+\varepsilon\frac{k_{dis_{yy}}}{k_f}\right)(1-\varepsilon^*)\frac{k_s}{k_f}}\left(\frac{h_v}{k_f}\right)} \tag{33}$$

Note that

$$\frac{D_i}{2}\left.\frac{dI_0(\lambda r)}{dr}\right|_{r=\frac{D_i}{2}} = \lambda\frac{D_i}{2}I_1\left(\lambda\frac{D_i}{2}\right) \tag{34}$$

$$\frac{D_i}{2}\left.\frac{dK_0(\lambda r)}{dr}\right|_{r=\frac{D_i}{2}} = -\lambda\frac{D_i}{2}K_1\left(\lambda\frac{D_i}{2}\right) \tag{35}$$

where $I_{0,1}$ are the modified I Bessel functions of the zeroth, first, respectively. Correspondingly, $K_{0,1}$ are also the modified K Bessel functions of the zeroth, first, respectively.

The combination of Eqs. (27) and (25) readily gives the temperature of the fluid phase in the porous medium region:

$$\frac{\langle T\rangle^{f}-T_w}{Dq_w/\left(k_{stag}+\varepsilon k_{dis_{yy}}\right)} = \frac{\left(k_{stag}+\varepsilon k_{dis_{yy}}\right)}{2\left(\varepsilon^* k_f+\varepsilon k_{dis_{yy}}\right)}\left[2J\left(\frac{r^2}{D^2}-\frac{1}{4}\right)+(1-J)\ln\frac{r}{D/2}\right]-\frac{(1-\varepsilon^*)k_s}{\varepsilon^* k_f+\varepsilon k_{dis_{yy}}} \times\left(L_1 I_0(\lambda r)+L_2 K_0(\lambda r)+M_1\left(\frac{r}{D}\right)^2+M_2\ln\frac{r}{D/2}+M_3\right) \tag{36}$$

Therefore, the temperature of fluid phase in the interface T_i can be subsequently obtained

$$\frac{T_i-T_w}{Dq_w/\left(k_{stag}+\varepsilon k_{dis_{yy}}\right)} = \frac{\left(k_{stag}+\varepsilon k_{dis_{yy}}\right)}{2\left(\varepsilon^* k_f+\varepsilon k_{dis_{yy}}\right)}\left[2J\left(\left(\frac{R_p}{2}\right)^2-\frac{1}{4}\right)+(1-J)\ln(R_p)\right]-\frac{(1-\varepsilon^*)k_s}{\varepsilon^* k_f+\varepsilon k_{dis_{yy}}} \times\left(L_1 I_0\left(\lambda\frac{D_i}{2}\right)+L_2 K_0\left(\lambda\frac{D_i}{2}\right)+M_1\left(\frac{R_p}{2}\right)^2+M_2\ln(R_p)+M_3\right) \tag{37}$$

The temperature profile in the clear fluid region may readily be achieved by integrating Eq. (18) with the boundary condition $\partial\langle T\rangle^{f}/\partial r|_{r=0} = 0$ and the temperature of fluid phase in the interface as

$$\frac{\langle T\rangle^{f}-T_w}{Dq_w/\left(k_{stag}+\varepsilon k_{dis_{yy}}\right)} = \frac{J\left(k_{stag}+\varepsilon k_{dis_{yy}}\right)}{k_f}\left[1+\frac{R_p^2}{16Da}\right] \times\left(\frac{r}{D}\right)^2-\frac{J\left(k_{stag}+\varepsilon k_{dis_{yy}}\right)}{16Dak_f}\left(\frac{r}{D}\right)^4+N \tag{38}$$

where

$$N = \frac{\left(k_{stag}+\varepsilon k_{dis_{yy}}\right)}{2\left(\varepsilon^* k_f+\varepsilon k_{dis_{yy}}\right)}\left[2J\left(\left(\frac{R_p}{2}\right)^2-\frac{1}{4}\right)+(1-J)\ln(R_p)\right] -\frac{(1-\varepsilon^*)k_s}{\varepsilon^* k_f+\varepsilon k_{dis_{yy}}}\left(L_1 I_0\left(\lambda\frac{D_i}{2}\right)+L_2 K_0\left(\lambda\frac{D_i}{2}\right)+M_1\left(\frac{R_p}{2}\right)^2 +M_2\ln(R_p)+M_3\right)-\frac{J\left(k_{stag}+\varepsilon k_{dis_{yy}}\right)}{k_f}\left[1+\frac{R_p^2}{16Da}\right]\left(\frac{R_p}{2}\right)^2 +\frac{J\left(k_{stag}+\varepsilon k_{dis_{yy}}\right)}{16Dak_f}\left(\frac{R_p}{2}\right)^4 \tag{39}$$

The corresponding Nusselt number may be evaluated from

$$Nu_D = \frac{q_w D}{\left(T_w-\langle T\rangle_B^{f}\right)k_f} = \frac{k_{stag}+\varepsilon k_{dis_{yy}}}{k_f}\frac{1}{\frac{8}{D^2}\int_0^{D/2}\left(\frac{T_w-\langle T\rangle^{f}}{q_w D/\left(k_{stag}+\varepsilon k_{dis_{yy}}\right)}\right)\frac{u}{u_B}r\,dr} \tag{40}$$

Xu et al. [24] obtained the Nussselt number for the case of ks/kf = 8200, Da = 1.5×10^{-4} and $\varepsilon = 0.95$. In Fig. 4, the present results of the Nusselt number based on the plug flow approximation are

compared with those obtained by Xu et al. with the Brinkman effects considered. The difference between the two sets of the results is indiscernible, as reported also by Yang et al. [36]. Thus, the plug flow approximation is quite effective to evaluate accurately the heat transfer rate from the wall covered with a porous medium layer. The case of fully filled porous medium ($R_p = 0$) yields the maximum Nusselt number, whereas the case of pure fluid ($R_p = 1$) gives its minimum. The Nusselt number decreases drastically for the case of partial filling, $R_p > 0.1$, since most fluid tends to flow through the core without a porous medium freely.

4.2. Local thermal equilibrium analysis

As for comparison, we also seek the temperature profile and Nusselt number based on the assumption of local thermal equilibrium model, namely, $\langle T\rangle^s = \langle T\rangle^f = T$. The temperature profile in the porous medium region, which satisfies the boundary condition as given by $q_w = (\varepsilon^* k_f + \varepsilon k_{dis_{yy}})(\partial\langle T\rangle^f/\partial r)|_{r=D/2} + (1-\varepsilon^*)k_s(\partial\langle T\rangle^s/\partial r)|_{r=D/2} = \text{const.}$, can readily be obtained as

$$\frac{T-T_w}{Dq_w/\left(k_{stag}+\varepsilon k_{dis_{yy}}\right)} = J\left[\left(\frac{r}{D}\right)^2-\frac{1}{4}\right]+\frac{1-J}{2}\ln\left(\frac{r}{D/2}\right) \tag{41}$$

Therefore, the temperature in the interface T_i can be subsequently achieved as

$$\frac{T_i-T_w}{Dq_w/\left(k_{stag}+\varepsilon k_{dis_{yy}}\right)} = J\left[\left(\frac{R_p}{2}\right)^2-\frac{1}{4}\right]+\frac{1-J}{2}\ln(R_p) \tag{42}$$

By integrating Eq. (18) with the boundary condition $\partial\langle T\rangle^f/\partial r|_{r=0} = 0$ and matching Eq. (42), the temperature profile in the clear fluid region may readily be obtained as

$$\frac{T-T_w}{Dq_w/\left(k_{stag}+\varepsilon k_{dis_{yy}}\right)} = \frac{4J\left(k_{stag}+\varepsilon k_{dis_{yy}}\right)}{k_f}\left[\frac{-1}{64Da}\left(\frac{r}{D}\right)^4+\left(1+\frac{R_p^2}{16Da}\right)\frac{(r/D)^2}{4}\right]+O \tag{43}$$

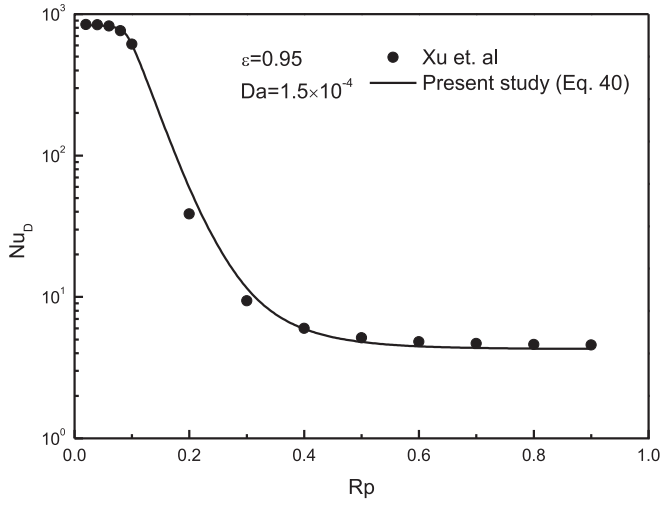

Fig. 4. Comparison of the present results based on the plug flow approximation with those of Xu et al.

where

$$O = J\left[\left(\frac{R_p}{2}\right)^2-\frac{1}{4}\right]+\frac{1-J}{2}\ln(R_p) - \frac{4J\left(k_{stag}+\varepsilon k_{dis_{yy}}\right)}{k_f}\left[\frac{-1}{64Da}\left(\frac{R_p}{2}\right)^4+\left(1+\frac{R_p^2}{16Da}\right)\frac{R_p^2}{16}\right] \tag{44}$$

Thus, the Nusselt number of our concern may be evaluated according to Eqs. (41) and (43) as

$$\begin{aligned}\frac{1}{Nu_D} &= -\frac{(T_B-T_w)k_f}{q_w D} \\ &= -\frac{k_f}{k_{stag}+\varepsilon k_{dis_{yy}}}\frac{8}{D^2}\int_0^{D/2}\left(\frac{T-T_w}{q_w D/\left(k_{stag}+\varepsilon k_{dis_{yy}}\right)}\right)\frac{u}{u_B}r\,dr \\ &= -\frac{8Jk_f}{k_{stag}+\varepsilon k_{dis_{yy}}}\left[\frac{O_1}{2048Da^2}\left(\frac{R_p}{2}\right)^8-\frac{5O_2O_1}{384Da}\left(\frac{R_p}{2}\right)^6 - \left(\frac{O}{Da}-O_2^2O_1\right)\left(\frac{R_p}{2}\right)^4/16+\frac{O_2O}{2}\left(\frac{R_p}{2}\right)^2 - \frac{J}{64}-\frac{1-J}{32}-J\left(\frac{1}{4}\left(\frac{R_p}{2}\right)^4-\frac{1}{8}\left(\frac{R_p}{2}\right)^2\right) - \frac{1-J}{2}\left(\frac{1}{2}\left(\frac{R_p}{2}\right)^2\ln(R_p)-\frac{1}{4}\left(\frac{R_p}{2}\right)^2\right)\right]\end{aligned} \tag{45}$$

where

$$O_1 = \frac{4J\left(k_{stag}+\varepsilon k_{dis_{yy}}\right)}{k_f} \tag{46}$$

and

$$O_2 = 1+\frac{R_p^2}{16Da} \tag{47}$$

Due to a number of advantages such as high thermal conductivity, high strength, large specific surface area and low density etc., aluminum foams are considered to be ideal porous media for possible engineering applications, such as compact heat exchangers, heat sinks for power electronics, condenser towers and regenerators. Calmidi and Mahajan [37,38] investigated the effective thermal conductivity, interstitial heat transfer coefficient and thermal dispersion, and proposed useful experimental correlations as follows:

$$\frac{k_{stag}}{k_f} = \varepsilon+0.19(1-\varepsilon)^{0.763}\sigma \tag{48}$$

$$\begin{aligned}Nu_v &= \frac{h_v d_m^2}{k_f} \\ &= 8.72(1-\varepsilon)^{1/4}\left(\frac{1-e^{-(1-\varepsilon)/0.04}}{\varepsilon}\right)^{1/2}\left(\frac{u_D d_m}{\nu}\right)^{1/2}Pr^{0.37}\end{aligned} \tag{49}$$

$$\frac{\varepsilon k_{dis_{yy}}}{k_f} = 0.06\left(\frac{\rho_f c_{p_f} u_D\sqrt{K}}{k_f}\right) \tag{50}$$

$$K/d_m^2 = 0.00073(1-\varepsilon)^{-0.224}\left(\frac{1.18}{1-e^{-(1-\varepsilon)/0.04}}\sqrt{\frac{1-\varepsilon}{3\pi}}\right)^{-1.11} \tag{51}$$

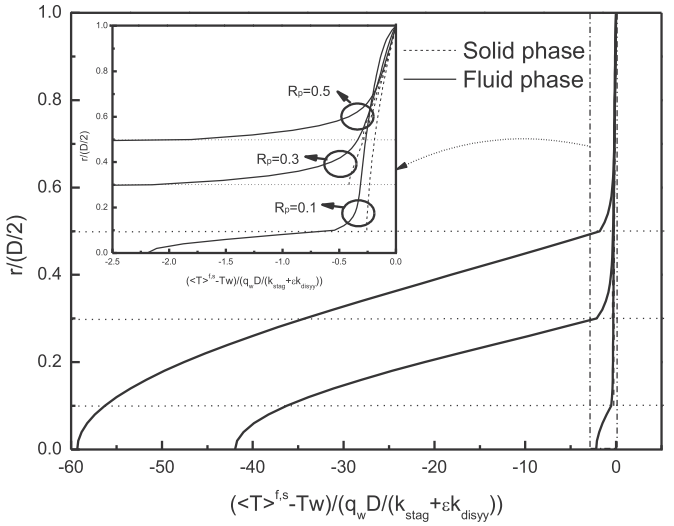

Fig. 5. Fluid and solid temperature profiles in a tube with its wall covered with a porous medium layer.

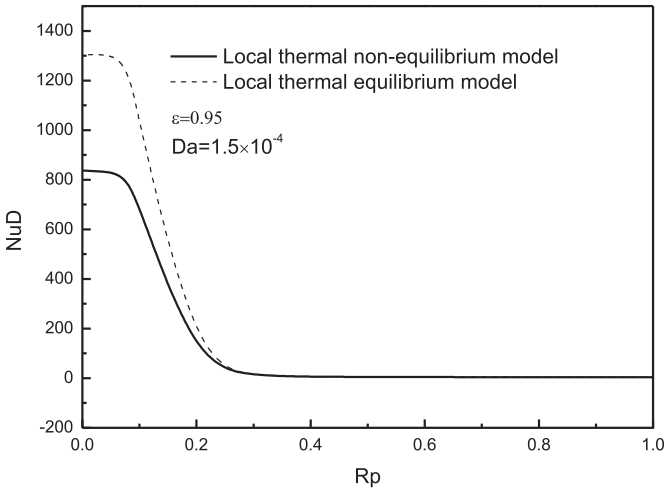

Fig. 6. Comparison of local thermal equilibrium and non-equilibrium analyses for forced convection with its wall covered with a porous medium layer.

where u_D is the Darcian velocity, σ is the ratio of thermal conductivity of solid phase to that of fluid phase, and d_m is the pore diameter.

Using these correlations for the case of aluminum foam and air combination, with $\sigma = 8200$, $\varepsilon = 0.95$, $\rho_f c_{p_f} u_D D/k_f = 5000$, $d_m/D = 0.1$ and $K/d_m^2 = 0.015$, both fluid and solid temperature profiles are generated from the foregoing local thermal non-equilibrium model and are presented in Fig. 5, assuming $\Delta T = 0$. Note that the stagnant thermal conductivity, the volumetric heat transfer coefficient and the dispersion coefficient, obtained based on Eqs. (48)–(51), are given by $k_{stag}/k_f = 160$, $\varepsilon k_{dis_{yy}}/k_f = 3.67$ and $\lambda D = 42.1$, respectively.

It can be clearly seen from Fig. 5, the solid temperature within the metal foam layer stays higher than that of the fluid phase, since the thermal conductivity of the metal foam is much higher than that of the air. This temperature difference within the wall layer significantly reflects on the level of the Nusselt number, as can be seen in Fig. 6, where the two curves generated from the local thermal equilibrium and non-equilibrium analyses are presented respectively. The figure indicates that the local thermal equilibrium analysis overestimates the Nusselt number, yielding significant errors especially for small R_p. Thus, we may conclude that the local thermal non-equilibrium must be used to evaluate the heat transfer rate through the metal foam layer.

5. Thermal analysis for forced convection in a tube with a porous medium core

Another possible way to enhance the heat transfer may be to place the porous cylinder in the core region of the tube, as proposed by many researchers including Liu et al. [39] and Yang et al. [22]. Yang et al. obtained approximate solutions under the local thermal equilibrium assumption. Since exact solutions have not been reported yet, neither under the local thermal equilibrium nor non-equilibrium assumption, we shall seek below exact solutions for both assumptions and compare these two sets of the results. The corresponding physical model is indicated in Fig. 1(b).

5.1. Velocity field

The velocity profile and friction factor for the case are given by Yang et al. [22] as

$$u = -\frac{K}{\mu_f}\frac{dp}{dx} \equiv u_i = \text{const.} \quad \text{for} \quad 0 \le r \le D_i/2 \tag{52}$$

$$u = 2u_i\left[\frac{1-(r/(D/2))^2}{32\text{Da}} + \left(1-\frac{1-R_p^2}{16\text{Da}}\right)\frac{\ln(r/(D/2))}{2\ln R_p}\right] \quad \text{for} \quad D_i/2 \le r \le D/2 \tag{53}$$

and

$$\lambda_f \equiv -\frac{2D}{\rho u_B^2}\frac{d\langle p\rangle^f}{dx} = \frac{64}{\text{Re}_D\left(1-R_p^4-\left(32\text{Da}-2\left(1-R_p^2\right)\right)\frac{1-R_p^2}{2\ln R_p}\right)} \tag{54}$$

where

$$J_1 \equiv \frac{u_i}{u_B} = \frac{1}{\frac{1-R_p^4}{32\text{Da}}-\left(1-\frac{1-R_p^2}{32\text{Da}}\right)\frac{1-R_p^2}{2\ln R_p}} \tag{55}$$

5.2. Local thermal non-equilibrium analysis

Following the same procedure as in the preceding case, the temperature profiles of both fluid and solid phases are obtained under the assumption of local thermal non-equilibrium.

For the solid phase in the core porous medium:

$$\frac{\langle T\rangle^s - T_w}{Dq_w/\left(k_{stag}+\varepsilon k_{dis_{yy}}\right)} = \frac{4J_1}{(\lambda D)^2}\left[1-\frac{I_0(\lambda r)}{I_0(\lambda D_i/2)}\right] + J_1\left[\left(\frac{r}{D}\right)^2-\left(\frac{R_p}{2}\right)^2\right]+Y \tag{56}$$

For the fluid phase in the core porous medium:

$$\frac{\langle T\rangle^{\mathrm{f}}-T_{\mathrm{w}}}{Dq_{\mathrm{w}}/\left(k_{\mathrm{stag}}+\varepsilon k_{\mathrm{dis}_{yy}}\right)}=\frac{J_1\left(k_{\mathrm{stag}}+\varepsilon k_{\mathrm{dis}_{yy}}\right)}{\varepsilon^{*}k_{\mathrm{f}}+\varepsilon k_{\mathrm{dis}_{yy}}}\left[\left(\frac{r}{D}\right)^2-\left(\frac{R_{\mathrm{p}}}{2}\right)^2\right]-\frac{(1-\varepsilon^{*})k_{\mathrm{s}}}{\varepsilon^{*}k_{\mathrm{f}}+\varepsilon k_{\mathrm{dis}_{yy}}}\left\{\frac{4J_1}{(\lambda D)^2}\left[1-\frac{I_0(\lambda r)}{I_0(\lambda D_{\mathrm{i}}/2)}\right]+J_1\left[\left(\frac{r}{D}\right)^2-\left(\frac{R_{\mathrm{p}}}{2}\right)^2\right]\right\}+Y \tag{57}$$

For the clear fluid region over the wall:

$$\frac{\langle T\rangle^{\mathrm{f}}-T_{\mathrm{w}}}{Dq_{\mathrm{w}}/\left(k_{\mathrm{stag}}+\varepsilon k_{\mathrm{dis}_{yy}}\right)}=\frac{J_1\left(k_{\mathrm{stag}}+\varepsilon k_{\mathrm{dis}_{yy}}\right)}{k_{\mathrm{f}}}\left[\frac{(r/D)^2-(r/D)^4-3/16}{16\mathrm{Da}}+\left(1-\frac{1-R_{\mathrm{p}}^2}{16\mathrm{Da}}\right)\frac{(r/D)^2(\ln(2r/D)-1)+1/4}{\ln(R_{\mathrm{p}})}\right]+\frac{k_{\mathrm{stag}}+\varepsilon k_{\mathrm{dis}_{yy}}}{k_{\mathrm{f}}}\left[\frac{1}{2}-\frac{J_1}{64\mathrm{Da}}+\left(1-\frac{1-R_{\mathrm{p}}^2}{16\mathrm{Da}}\right)\times\frac{J_1}{4\ln(R_{\mathrm{p}})}\right]\ln(2r/D) \tag{58}$$

where

$$\begin{aligned}Y&=\frac{T_{\mathrm{i}}-T_{\mathrm{w}}}{Dq_{\mathrm{w}}/\left(k_{\mathrm{stag}}+\varepsilon k_{\mathrm{dis}_{yy}}\right)}\\&=\frac{J_1\left(k_{\mathrm{stag}}+\varepsilon k_{\mathrm{dis}_{yy}}\right)}{k_{\mathrm{f}}}\left[\frac{R_{\mathrm{p}}^2/4-R_{\mathrm{p}}^4/16-3/16}{16\mathrm{Da}}+\left(1-\frac{1-R_{\mathrm{p}}^2}{16\mathrm{Da}}\right)\frac{R_{\mathrm{p}}^2/4(\ln(R_{\mathrm{p}})-1)+1/4}{\ln(R_{\mathrm{p}})}\right]+\frac{k_{\mathrm{stag}}+\varepsilon k_{\mathrm{dis}_{yy}}}{k_{\mathrm{f}}}\left[\frac{1}{2}-\frac{J_1}{64\mathrm{Da}}+\left(1-\frac{1-R_{\mathrm{p}}^2}{16\mathrm{Da}}\right)\times\frac{J_1}{4\ln(R_{\mathrm{p}})}\right]\ln(R_{\mathrm{p}})\end{aligned} \tag{59}$$

The corresponding Nusselt number could be evaluated by Eq. (40).

5.3. Local thermal equilibrium analysis

It is rather straightforward to show that under the local thermal equilibrium model, the temperature profile in the clear fluid region over the wall is given by

$$\frac{T-T_{\mathrm{w}}}{Dq_{\mathrm{w}}/\left(k_{\mathrm{stag}}+\varepsilon k_{\mathrm{dis}_{yy}}\right)}=Z_1\ln\left(\frac{r}{D/2}\right)+Z_2+\frac{J_1\left(k_{\mathrm{stag}}+\varepsilon k_{\mathrm{dis}_{yy}}\right)}{k_{\mathrm{f}}}\left[\frac{\left(\frac{r}{D}\right)^2-\left(\frac{r}{D}\right)^4}{16\mathrm{Da}}+\left(1-\frac{1-R_{\mathrm{p}}^2}{16\mathrm{Da}}\right)\frac{\left(\frac{r}{D}\right)^2\ln\left(\frac{r}{D/2}\right)-\left(\frac{r}{D}\right)^2}{\ln R_{\mathrm{p}}}\right] \tag{60}$$

where

$$Z_1=\frac{k_{\mathrm{stag}}+\varepsilon k_{\mathrm{dis}_{yy}}}{2kf}\left[1+\frac{J_1}{32\mathrm{Da}}-\left(1-\frac{1-R_{\mathrm{p}}^2}{16\mathrm{Da}}\right)\frac{J_1}{2\ln R_{\mathrm{p}}}\right] \tag{61}$$

$$Z_2=\frac{J_1\left(k_{\mathrm{stag}}+\varepsilon k_{\mathrm{dis}_{yy}}\right)}{kf}\left[\left(1-\frac{1-R_{\mathrm{p}}^2}{16\mathrm{Da}}\right)\frac{1}{4\ln R_{\mathrm{p}}}-\frac{3}{256\mathrm{Da}}\right] \tag{62}$$

Therefore, the temperature in the interface T_{i} can be subsequently achieved as

$$\frac{T_{\mathrm{i}}-T_{\mathrm{w}}}{Dq_{\mathrm{w}}/\left(k_{\mathrm{stag}}+\varepsilon k_{\mathrm{dis}_{yy}}\right)}=Z_1\ln R_{\mathrm{p}}+Z_2+\frac{J_1\left(k_{\mathrm{stag}}+\varepsilon k_{\mathrm{dis}_{yy}}\right)}{k_{\mathrm{f}}}\times\left[\frac{\left(\frac{R_{\mathrm{p}}}{2}\right)^2-\left(\frac{R_{\mathrm{p}}}{2}\right)^4}{16\mathrm{Da}}+\left(1-\frac{1-R_{\mathrm{p}}^2}{16\mathrm{Da}}\right)\times\frac{\left(\frac{R_{\mathrm{p}}}{2}\right)^2\ln R_{\mathrm{p}}-\left(\frac{R_{\mathrm{p}}}{2}\right)^2}{\ln R_{\mathrm{p}}}\right]=Z \tag{63}$$

By integrating Eq. (24) with the boundary condition $\partial\langle T\rangle^{f}/\partial r|_{r=0}=0$ and matching Eq. (63), the temperature profile in the porous medium of the core region may readily be obtained as

$$\frac{T-T_{\mathrm{w}}}{Dq_{\mathrm{w}}/\left(k_{\mathrm{stag}}+\varepsilon k_{\mathrm{dis}_{yy}}\right)}=J_1\left[\left(\frac{r}{D}\right)^2-\frac{R_{\mathrm{p}}^2}{4}\right]+Z \tag{64}$$

Hence, the corresponding Nusselt number may be given by

$$\begin{aligned}\frac{1}{\mathrm{Nu}_D}&=-\frac{(T_{\mathrm{B}}-T_{\mathrm{w}})k_{\mathrm{f}}}{q_{\mathrm{w}}D}=-\frac{k_{\mathrm{f}}}{k_{\mathrm{stag}}+\varepsilon k_{\mathrm{dis}_{yy}}}\times\frac{8}{D^2}\int_0^{D/2}\left(\frac{T-T_{\mathrm{w}}}{q_{\mathrm{w}}D/\left(k_{\mathrm{stag}}+\varepsilon k_{\mathrm{dis}_{yy}}\right)}\right)\frac{u}{u_{\mathrm{B}}}r\,\mathrm{d}r\\&=-\frac{8J_1k_{\mathrm{f}}}{k_{\mathrm{stag}}+\varepsilon k_{\mathrm{dis}_{yy}}}\left\{\frac{ZR_{\mathrm{p}}^2}{8}-\frac{R_{\mathrm{p}}^4}{64}J_1+\frac{J_1\left(k_{\mathrm{stag}}+\varepsilon k_{\mathrm{dis}_{yy}}\right)}{k_{\mathrm{f}}}\left[\frac{\frac{1}{4}\frac{1-R_{\mathrm{p}}^4}{2^4}-\frac{5}{6}\frac{1-R_{\mathrm{p}}^6}{2^6}+\frac{1}{2}\frac{1-R_{\mathrm{p}}^8}{2^8}}{256\mathrm{Da}^2}+Z_3\frac{2Z_4-5Z_5-\frac{1}{4}\frac{1-R_{\mathrm{p}}^4}{2^4}+\frac{2}{3}\frac{1-R_{\mathrm{p}}^6}{2^6}}{16\mathrm{Da}\ln R_{\mathrm{p}}}+Z_3^2\frac{Z_6-Z_4}{(\ln R_{\mathrm{p}})^2}\right]\right.\\&\quad+\frac{Z_1}{16\mathrm{Da}}(Z_7-4Z_4)+\frac{Z_1Z_3}{\ln R_{\mathrm{p}}}Z_8\\&\quad\left.+Z_2\frac{\frac{1}{2}\frac{1-R_{\mathrm{p}}^2}{2^2}-\frac{1-R_{\mathrm{p}}^4}{2^4}}{16\mathrm{Da}}+Z_2Z_3\frac{Z_7}{\ln R_{\mathrm{p}}}\right\}\end{aligned} \tag{65}$$

where

$$Z_3=1-\frac{1-R_{\mathrm{p}}^2}{16\mathrm{Da}} \tag{66}$$

$$Z_4=\int_{D_{\mathrm{i}}/2}^{D/2}\frac{r^3}{D^4}\ln\frac{r}{D/2}\mathrm{d}r=\frac{R_{\mathrm{p}}^4-1}{256}-\frac{R_{\mathrm{p}}^4\ln R_{\mathrm{p}}}{64} \tag{67}$$

$$Z_5=\int_{D_{\mathrm{i}}/2}^{D/2}\frac{r^5}{D^6}\ln\frac{r}{D/2}\mathrm{d}r=\frac{R_{\mathrm{p}}^6-1}{2304}-\frac{R_{\mathrm{p}}^6\ln R_{\mathrm{p}}}{384} \tag{68}$$

$$Z_6 = \int_{D_i/2}^{D/2} \frac{r^3}{D^4}\left(\ln\frac{r}{D/2}\right)^2 dr = \frac{1-R_p^4}{512} - \frac{R_p^4(\ln R_p)^2}{64} + \frac{R_p^4 \ln R_p}{128} \quad (69)$$

$$Z_7 = \int_{D_i/2}^{D/2} \frac{r}{D^2}\ln\frac{r}{D/2} dr = \frac{R_p^2-1}{16} - \frac{R_p^2 \ln R_p}{8} \quad (70)$$

$$Z_8 = \int_{D_i/2}^{D/2} \frac{r}{D^2}\left(\ln\frac{r}{D/2}\right)^2 dr = \frac{1-R_p^2}{16} - \frac{R_p^2(\ln R_p)^2}{8} + \frac{R_p^2 \ln R_p}{8} \quad (71)$$

In Fig. 7, the results based on both local thermal equilibrium and non-equilibrium analyses are presented together in terms of the Nusselt number. For this particular case of having a porous medium in the core, the solid and fluid phases in the core region are virtually under local thermal equilibrium, since the porous core is isolated from the heated wall surface and saturated by the fluid. Thus, as can be seen from the figure, the difference between the two sets of the results is hardly discernible.

The Nusselt number stays at the lowest level for the case of pure fluid, and increases as placing the porous medium in the core region. On the contrary to the preceding case of having a porous layer over the wall, the increase in the Nusselt number with R_p is rather gradual, since the velocity increase over the heated wall, due to the insertion of the porous medium core, naturally leads to heat transfer enhancement.

6. Heat transfer performance assessment

In what follows, we shall compare the results obtained for the case of having a porous layer over the wall with those obtained for the case of a porous medium core, in order to find out which placement is preferred in view of heat transfer enhancement.

The variations of Nusselt number are presented in Fig. 8, where the Nusselt number is plotted against the same porous medium filling ratio, namely, $A_p/A = 1 - R_p^2$ for the case of having a porous layer over the wall, and $A_p/A = R_p$ for the case of a porous medium core.

The figure clearly indicates that more we fill the porous medium (either over the wall or core), the higher Nusselt number we get. Its increase is gradual for the case of a porous medium core, whereas it is steep toward $A_p/A = 1$ for the case of a porous medium layer on the wall. For the same A_p/A, the Nusselt number for the case of a porous medium core is always higher than that for the case of a porous medium layer on the wall. The corresponding friction coefficients are plotted in Fig. 9, in a similar fashion. The figure shows that, for fixed Reynolds number and porous medium filling ratio, the case of a porous medium core always yields more flow resistance than the case of a porous medium layer on the wall. Thus, the case of a porous medium core gives more heat transfer at expense of more flow resistance.

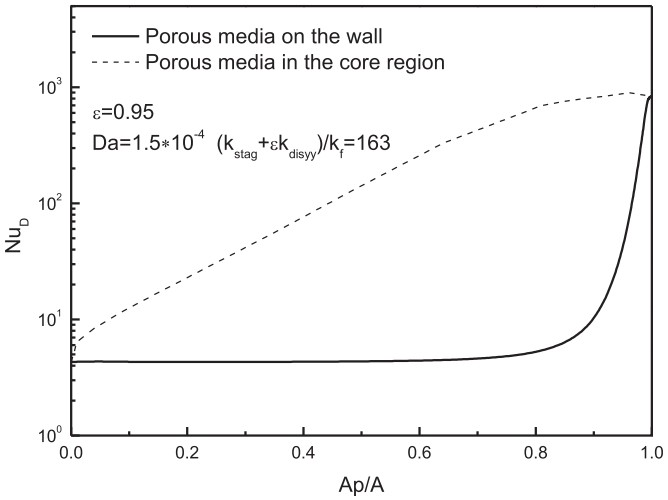

Fig. 8. Effect of porous medium filling on Nusselt number.

In order to make a rational heat transfer enhancement assessment, the results of the Nusselt number for the case of $A_p/A = 0.99$, namely, $R_p = 0.1$ for the tube with its wall covered by a porous medium layer and $R_p = 0.995$ for the tube with a porous medium core, are re-plotted in Fig. 10 against the dimensionless pumping power as defined by

$$\text{P.P.} = \lambda_f^{1/3}\text{Re} \quad (72)$$

It is interesting to note that, in the range of comparatively low pumping power, the Nusselt number for the case of a porous

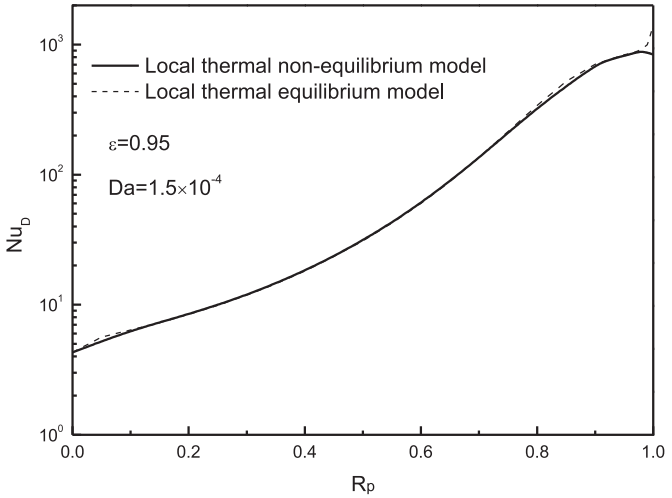

Fig. 7. Comparison of local thermal equilibrium and non-equilibrium analyses for forced convection in a tube with a porous medium core.

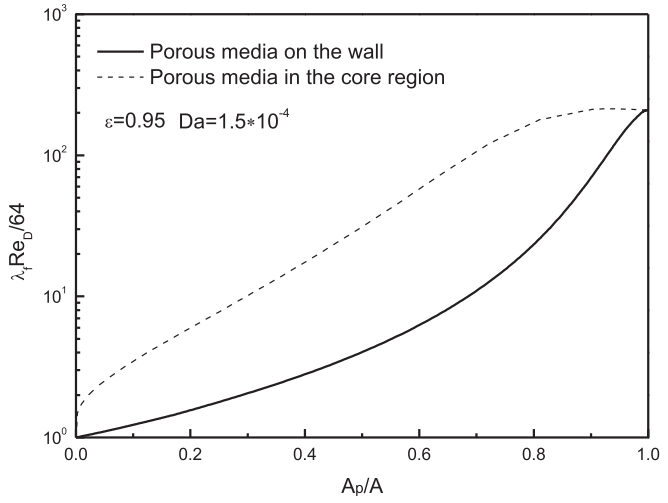

Fig. 9. Effect of porous medium filling on friction factor.

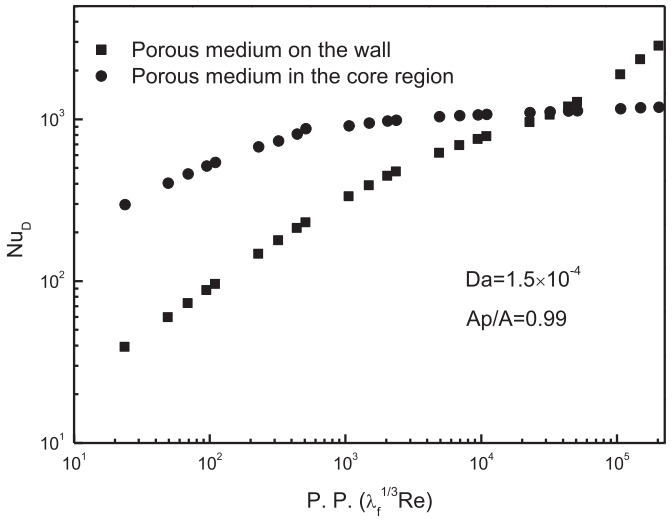

Fig. 10. Comparison of Nusselt number under equal pumping power.

medium core is higher than that for the case of a porous medium layer on the wall, whereas, in the range of high pumping power, that the latter exceeds the former. Therefore, for given operating conditions, a careful examination is required to find out which placement is better in view of heat transfer enhancement.

7. Conclusions

In this study, theoretical analyses were made to investigate forced convection in a tube with a porous medium core and a tube with a wall covered with a porous medium layer. Both thermal and non-thermal equilibrium analyses were carried out for these two cases to investigate the validity of local thermal equilibrium assumption. It was found that the local thermal non-equilibrium analysis is essential for the case of forced convection in a tube with a heated wall surface covered with a porous medium layer, whereas the local thermal equilibrium analysis suffices to capture transport phenomena for the case of forced convection in a tube with a porous medium core. An assessment was made in view of heat transfer enhancement under equal pumping power, which reveals that, in a low range of pumping power, the heat transfer performance of the tube with a porous medium core is higher than that of the tube with a wall covered with a porous medium layer. However, in a high range of pumping power, the latter performance exceeds the former.

Acknowledgments

This work has been partially supported by the National Natural Science Foundation of China (No. 51036003).

References

[1] A.V. Kuznetsov, Analytical studies of forced convection in partly porous configurations. in: K. Vafai (Ed.), Handbook of Porous Media. Marcel Dekker, New York, 2000, pp. 269–312.
[2] N. Dukhan, R. Picon-Feliciano, A.R. Alvarez-Hernandez, Heat transfer analysis in metal foams with low conductivity fluids, J. Heat Transf. 128 (2006) 784–792.
[3] D. Poulikakos, M. Kazmierczak, Forced convection in a duct partially filled with a porous material, J. Heat Transf. 109 (1987) 653–662.
[4] W.J. Minkowycz, A. Haji-Sheikh, K. Vafai, On departure from local thermal equilibrium in porous media due to a rapidly changing heat source: the Sparrow number, Int. J. Heat Mass Transf. 42 (1999) 3373–3385.
[5] S.J. Kim, S.P. Jang, Effects of the Darcy number, the Prandtl number, and the Reynolds number on local thermal non-equilibrium, Int. J. Heat Mass Transf. 45 (2002) 3885–3896.
[6] M.A. Al-Nimr, B. Abu-Hijleh, Validation of thermal equilibrium assumption in transient forced convection flow in porous channel, Transport Porous Media 49 (2002a) 1–8.
[7] M.A. Al-Nimr, S. Kiwan, Examination of the thermal equilibrium assumption in periodic forced convection in a porous channel, J. Porous Media 5 (2002b) 35–40.
[8] B.A. Abu-Hijleh, M.A. Al-Nimr, M.A. Hader, Thermal equilibrium in transient forced convection flow in porous channel, Transport Porous Media 49 (2002) 127–138.
[9] X.W. Zhang, W. Liu, Z.C. Liu, Criterion for local thermal equilibrium in forced convection flows through porous media, J. Porous Media 12 (2009) 1103–1111.
[10] X.W. Zhang, W. Liu, Thermal non-equilibrium modeling of coupled heat and mass transfer in bulk adsorption system of porous media, J. Porous Media 14 (2011) 555–563.
[11] S. Khashan, M.A. Al-Nimr, Validation of the local thermal equilibrium assumption in forced convection of non-Newtonian fluids through porous channels, Transport Porous Media 61 (2005) 291–305.
[12] S. Khashan, A.M. Al-Amiri, M.A. Al-Nimr, Assessment of the local thermal non-equilibrium condition in developing forced convection flows through fluid-saturated porous tubes, Appl. Therm. Eng. 25 (2005) 1429–1445.
[13] D.A. Nield, A. Bejan, Convection in Porous Media, third ed. Springer, New York, 2006, pp. 86–87.
[14] M.K. Alkam, M.A. Al-Nimr, Improving the performance of double-pipe heat exchangers by using porous substrates, Int. J. Heat Mass Transf. 42 (1999) 3609–3618.
[15] M.A. Al-Nimr, M.K. Alkam, Unsteady non-Darcian fluid flow in parallel plates channels partially filled with porous materials, Heat Mass Transf. 33 (1998) 315–318.
[16] M.K. Alkam, M.A. Al-Nimr, M.O. Hamdan, Enhancing heat transfer in parallel-plate channels by using porous inserts, Int. J. Heat Mass Transf. 44 (2001) 931–938.
[17] M.K. Alkam, M.A. Al-Nimr, M.O. Hamdan, On forced convection in channels partially filled with porous substrates, Heat Mass Transf. 38 (2002) 337–342.
[18] A. Nakayama, F. Kuwahara, M. Sugiyama, G. Xu, A two-energy equation model for conduction and convection in porous media, Int. J. Heat Mass Transf. 44 (2001) 4375–4379.
[19] C.T. Hsu, Heat conduction in porous media. in: K. Vafai (Ed.), Handbook of Porous Media. Marcel Dekker, New York, 2000, pp. 170–200.
[20] C.T. Hsu, P. Cheng, K.W. Wong, A lumped parameter model for stagnant thermal conductivity of spatially periodic porous media, ASME Trans. J. Heat Transf. 117 (1995) 264–269.
[21] T.W. Tong, M.C. Sharatchandra, Z. Gdoura, Using porous inserts to enhance heat transfer in laminar fully-developed flows, Int. Comm. Heat Mass Transf. 20 (1993) 761–770.
[22] C. Yang, W. Liu, A. Nakayama, Forced convective heat transfer enhancement in a tube with its core partially filled with a porous medium, Open Transport Phenom. 1 (2009) 1–6.
[23] D. Bhargavi, V.V. Satyamurty, Optimum porous insert configurations for enhanced heat transfer in channels, J. Porous Media 10 (2011) 187–203.
[24] H.J. Xu, Z.G. Qu, W.Q. Tao, Analytical solution of forced convective heat transfer in tubes partially filled with metallic foam using the two-equation model, Int. J. Heat Mass Transf. 54 (2011) 3846–3855.
[25] B.I. Pavel, A.A. Mohamad, An experimental and numerical study on heat transfer enhancement for gas heat exchangers fitted with porous media, Int. J. Heat Mass Transf. 47 (2004) 4939–4952.
[26] B.I. Pavel, A.A. Mohamad, Experimental investigation of the potential of metallic porous insert in enhancing forced convective heat transfer, ASME J. Heat Transf. 126 (2004) 540–545.
[27] A.A. Mohamad, Heat transfer enhancements in heat exchangers fitted with porous media, part I: constant wall temperature, Int. J. Thermal Sci. 42 (2003) 385–395.
[28] Z.F. Huang, A. Nakayama, K. Yang, C. Yang, W. Liu, Enhancing heat transfer in the core flow by using porous medium insert in a tube, Int. J. Heat Mass Transf. 53 (2010) 1164–1174.
[29] M. Quintard, S. Whitaker, One and two equation models for transient diffusion processes in two-phase systems, Adv. Heat Transf. 23 (1993) 369–465.
[30] M. Quintard, S. Whitaker, Local thermal equilibrium for transient heat conduction: theory and comparison with numerical experiments, Int. J. Heat Mass Transf. 38 (1995) 2779–2796.
[31] P. Cheng, Heat transfer in geothermal systems, Adv. Heat Transf. 14 (1978) 1–105.
[32] A. Nakayama, PC-Aided Numerical Heat Transfer and Convective Flow. CRC Press, Boca Raton, 1995, pp. 49–50, 103–115.
[33] C. Yang, A. Nakayama, A synthesis of tortuosity and dispersion in effective thermal conductivity of porous media, Int. J. Heat Mass Transf. 53 (2010) 3222–3230.
[34] A. Nakayama, F. Kuwahara, Y. Kodama, An equation for thermal dispersion flux transport and its mathematical modelling for heat and fluid flow in a porous medium, J. Fluid Mech. 563 (2006) 81–96.
[35] Y.L. Jamin, A.A. Mohamad, Enhanced heat transfer using porous carbon foam in cross flow, J. Heat Transf. 129 (2007) 735–742.

[36] C. Yang, K. Ando, A. Nakayama, A local thermal non-equilibrium analysis of fully developed forced convective flow in a tube filled with a porous medium, Transport Porous Media 89 (2011) 237–249.
[37] V.V. Calmidi, R.L. Mahajan, The effective thermal conductivity of high porosity fibrous metal foams, ASME Trans. J. Heat Transf. 121 (1999) 466–471.
[38] V.V. Calmidi, R.L. Mahajan, Forced convection in high porosity metal foams, ASME Trans. J. Heat Transf. 122 (2000) 557–565.
[39] W. Liu, K. Yang, Mechanism and numerical analysis of heat transfer enhancement in the core flow along a tube, Sci. China, Ser E 51 (2008) 1195–1202.

Nomenclature

A: surface area (m^2)
A_{int}: interface between the fluid and solid (m^2)
c: specific heat (J/kg K)
c_p: specific heat at constant pressure (J/kg K)
D: tube diameter (m)
D_i: inner diameter (m)
Da: Darcy number (−)
d_m: mean pore diameter (m)
h_v: volumetric heat transfer coefficient (W/m^3 K)
k: thermal conductivity (W/m K)
K: permeability (m^2)
n_j: unit vector pointing outward from the fluid side to solid side (−)
Pr: Prandtl number (−)
q: heat flux (W/m^2)
r: radial coordinate
T: temperature (K)
u_D: Darcian velocity (uniform inlet velocity) (m/s)
u_i: velocity vector (m/s)
V: representative elementary volume (m^3)
x_i: Cartesian coordinates (m)
x, y, z: Cartesian coordinates (m)
ε: porosity (−)
ε^*: effective porosity (−)
ν: kinematic viscosity (m^2/s)
ρ: density (kg/m^2)
σ: ratio of thermal conductivity of solid phase to that of fluid phase (−)

Special symbols
$\tilde{\phi}$: deviation from intrinsic average
$\langle\phi\rangle$: Darician average
$\langle\phi\rangle^{f,s}$: intrinsic average

Subscripts and superscripts
dis: dispersion
f: fluid
s: solid
stag: stagnation
w: inner wall